Inorganic Chemistry

ARTICLE

pubs.acs.org/IC

"Covalent Hydration" Reactions in Model Monomeric Ru 2,2′-Bipyridine Complexes: Thermodynamic Favorability as a Function of Metal Oxidation and Overall Spin States

Abdullah Ozkanlar,* Jonathan L. Cape, James K. Hurst, and Aurora E. Clark*

Department of Chemistry, Washington State University, Pullman, Washington 99164, United States

Supporting Information

ABSTRACT: Density functional theory (DFT) has been used to investigate the plausibility of water addition to the simple mononuclear ruthenium complexes, $[(NH_3)_3(bpy)Ru{=}O]^{2+/3+}$ and $[(NH_3)_3(bpy)RuOH]^{3+}$, in which the OH fragment adds to the 2,2′-bipyridine (bpy) ligand. Activation of bpy toward water addition has frequently been postulated within the literature, although there exists little definitive experimental evidence for this type of "covalent hydration". In this study, we examine the energetic dependence of the reaction upon metal oxidation state, overall spin state of the complex, as well as selectivity for various positions on the bipyridine ring. The thermodynamic favorability is found to be highly dependent upon all three parameters, with free energies of reaction that span favorable and unfavorable regimes. Aqueous addition to $[(NH_3)_3(bpy)Ru{=}O]^{3+}$ was found to be highly favorable for the $S = 1/2$ state, while reduction of the formal oxidation state on the metal center makes the reaction highly unfavorable. Examination of both facial and meridional isomers reveals that when bipyridine occupies the position trans to the ruthenyl oxo atom, reactivity toward OH addition decreases and the site preferences are altered. The electronic structure and spectroscopic signatures (EPR parameters and simulated spectra) have been determined to aid in recognition of "covalent hydration" in experimental systems. EPR parameters are found to uniquely characterize the position of the OH addition to the bpy as well as the overall spin state of the system.

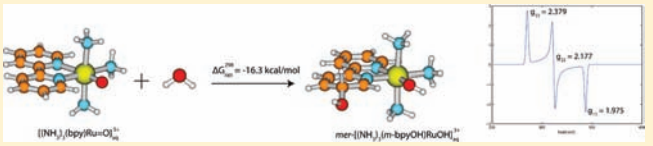

INTRODUCTION

The notion that metal-ion coordination might activate 2,2′-bipyridine (bpy) and related polyimines toward addition of water across N=C bonds was introduced in the 1970s by Gillard and co-workers to explain unusual spectroscopic and kinetic properties observed for complex ions containing these ligands.[1] These "covalent hydration" reactions were patterned after analogous reactions of nitrogen heterocyclic compounds that had been extensively studied by physical organic chemists.[2] However, no direct evidence could be found in subsequent research for predicted ligand symmetry reductions or OH addition to the heterocyclic ring in these coordination complexes. Several alternative explanations for their anomalous properties were advanced, including formation of monodentate intermediates, expansion of the metal coordination sphere, tight ion pairing, and carbanion formation.[3]

These considerations notwithstanding, one set of reactions that may be initiated by covalent hydration is the hydroxide-dependent reduction of group 8 $M(bpy)_3^{3+}$ ions.[4,5] In homogeneous solutions, these reactions involve primarily ligand degradation.[5,6] However, it has been reported that when encapsulated within a zeolite cage, $Ru(bpy)_3^{3+}$ undergoes one-electron reduction with quantitative release of O_2 via the reaction $4Ru(bpy)_3^{3+} + 2OH^- \rightarrow 4Ru(bpy)_3^{2+} + O_2 + 2H^+$.[7] Spectroscopic and EPR evidence suggesting intermediary OH addition to the ring were obtained. More recently, this model has been adapted to rationalize an unusual reaction pathway for water oxidation catalyzed by dimeric μ-oxo-bridged ruthenium ions ($[Ru^{III}(L)_2(OH_2)]_2O^{4+}$, L = 2,2′-bipyridine or a ring-substituted congener) which[18]O-isotope-labeling studies have identified as involving O_2 formation from two solvent molecules, as opposed to the coordinated aqua ligands.[8,9] The active form of this catalyst is a $4e^-$-oxidized species containing a diruthenyl ($Ru^V(O){-}O{-}Ru^V(O)$) core[10,11] that we proposed initiates water oxidation by H-atom abstraction; the nascent hydroxyl radical then undergoes concerted addition to either the adjacent Ru=O group to form a hydroperoxy/hydroxyl intermediate ($[L_2Ru^{IV}(OOH){-}O{-}Ru^{IV}(OH)L_2]^{n+}$) or the bipyridine ligand to form a ligand radical intermediate (for example, $[L_2Ru^{IV}(OH){-}O{-}Ru^V(OH)L(LOH^\bullet)]^{n+}$), which then decomposes to give an isotopically distinct O_2 molecule. Provisional support for this model includes detection of anomalous optical and EPR signals during catalytic turnover that appear consistent with OH addition to the ring[12] as well as demonstration that radiolytically generated hydroxyl radical adds to the bipyridine ring.[13] Theoretical support for the reaction model has been presented in the form of DFT calculations, confirming the presence of a low-energy pathway through the hydroperoxy/hydroxyl intermediate.[14] The proposed pathway involving ligand radical formation is largely

Received: March 29, 2011
Published: August 10, 2011

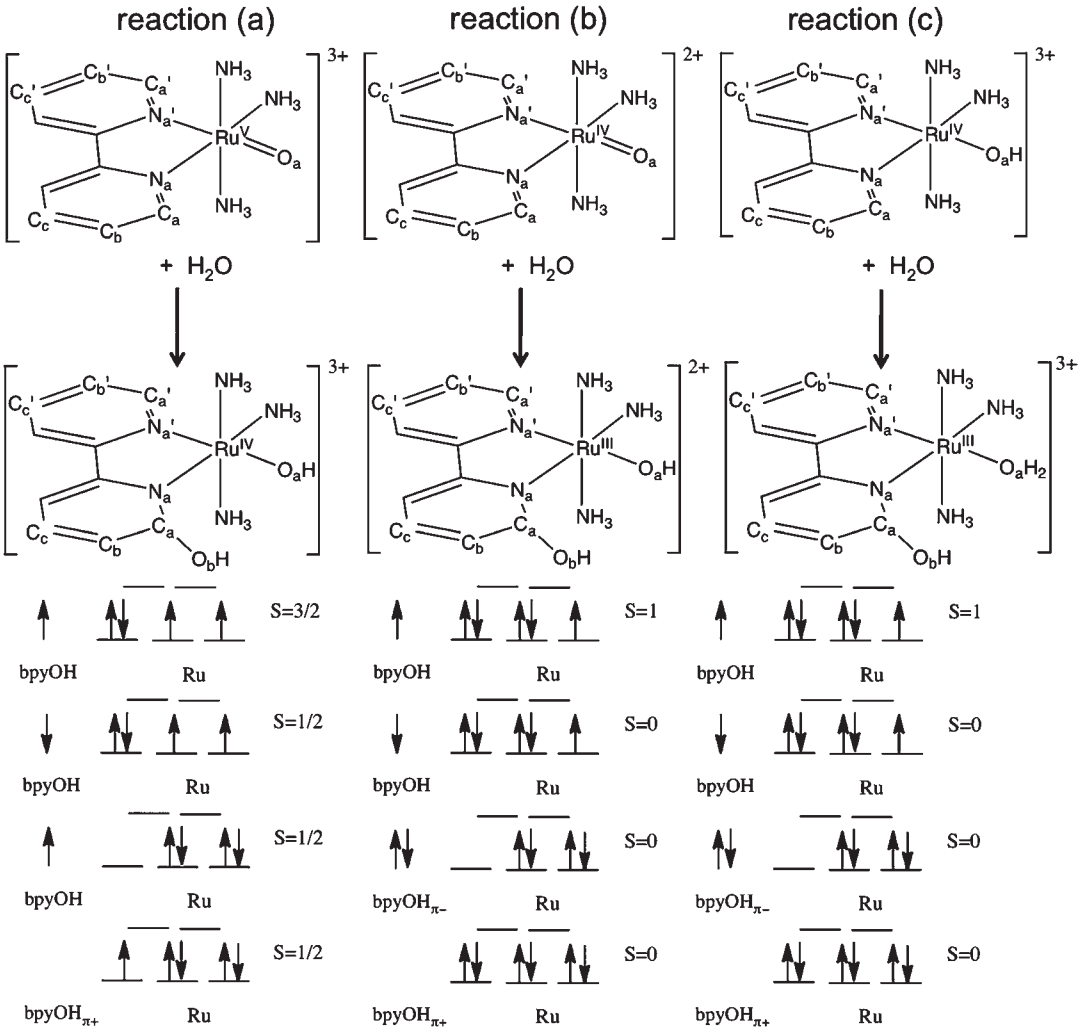

Figure 1. Reactions a−c of the meridional isomers of $[(NH_3)_3(bpy)Ru{=}O]^{3+}$, $[(NH_3)_3(bpy)Ru{=}O]^{2+}$, and $[(NH_3)_3(bpy)RuOH]^{3+}$ examined in this work, with product spin states studied and atom numbering indicated by subscripts. Water addition to only the ortho position (atom label C_a) shown for clarity.

unexplored from a theoretical perspective. However, in a very recent theoretical analysis of water oxidation catalyzed by the $[(tpy)(bpz)Ru^{IV}{=}O]^{2+}$ion (tpy = 2,2′:6′2″-terpyridine; bpz = 2,2′-bipyrazine) an energetically permissible pathway leading to OH addition to the terpyridine ligand was found.[15]

In the present study, we utilize density functional theory (DFT) to explore the plausibility of water addition to the fac and mer isomers of simple mononuclear ruthenium complexes ($[(NH_3)_3(bpy)Ru{=}O]^{2+/3+}$ and $[(NH_3)_3(bpy)Ru{-}OH]^{3+}$), in which reactivity is restricted to the pathway involving "covalent hydration" of the bipyridine ligand, including considerations of energetic dependencies upon the metal oxidation state, overall spin state of the complex, and selectivity for various positions on the bipyridine ring. Moreover, we identify key electronic structure and spectroscopic signatures to aid in future identification of these reactions. These model complexes are structurally similar to $[(tpy)(bpm)Ru{=}O]^{2+/3+}$ and $[(tpy)(bpz)Ru{=}O]^{2+/3+}$ (bpm = 2,2′-bipyrimidine; bpz = 2,2′-bipyrazine) mononuclear catalysts,[16,17] although we recognize that the presence of the hard NH_3 ligands in the model may restrict electron delocalization over the nuclear framework of the complex. A common feature of homogeneous water oxidation reactions catalyzed by polyimine-containing complexes, particularly when excess oxidants are present, is competitive oxidative degradation that can inactivate the catalyst after only a few reaction cycles.[18] These reactions can reasonably be expected to involve hydrolytic attack of water on reaction intermediates.[6] Thus, this study provides information that is useful both to evaluating proposed mechanisms and interpreting experimental data in water oxidation catalyzed by the dinuclear ruthenium complexes and to the design of more robust catalysts in general.

COMPUTATIONAL METHODS

The structures of the fac and mer isomers of $S = 3/2$ $[(NH_3)_3(bpy)Ru{=}O]^{3+}$ as well as the $S = 1$ spin states of $[(NH_3)_3(bpy)Ru{=}O]^{2+}$ and $[(NH_3)_3(bpy)RuOH]^{3+}$ reactants were optimized with the unrestricted B3LYP combination of density functionals[19] using the LANL2 effective core potential on Ru with the corresponding LANL2DZ basis set and the aug-cc-pVDZ basis on all main group elements (Figure 1).[20,21] All geometry optimizations were performed using the NWChem program package.[22] The potential products from water addition to the bpy ligand of $S = 3/2$ $[(NH_3)_3(bpy)Ru{=}O]^{3+}$ include $[(NH_3)_3(bpyOH)RuOH]^{3+}$ for which 5 different spin

dx.doi.org/10.1021/ic200646h |Inorg. Chem. 2011, 50, 8177–8187

Table 1. Key Bond Lengths (in Å) for Species in Reaction a Illustrated in Figure 1 As Calculated by B3LYP/LANL2DZ/aug-cc-pVDZ[a]

species	S	$r_{Ru-N_a'}$	r_{Ru-N_a}	$r_{N_a'-C_a'}$	$r_{N_a-C_a}$	r_{Ru-O_a}	$r_{C^*-O_b}$	$r_{O_a-O_b}$	$\langle r_{C-C^*}\rangle$
$[A_3(bpy)Ru{=}O]^{3+}$	3/2	2.28	2.11	1.33	1.33	1.77	NA	NA	NA
$[A_3(o\text{-bpyOH})RuOH]^{3+}$	3/2	2.12	2.10	1.35	1.47	1.86	1.45	2.60	NA
$[A_3(m\text{-bpyOH})RuOH]^{3+}$	3/2	2.08	2.10	1.36	1.31	1.88	1.43	4.90	1.50
$[A_3(p\text{-bpyOH})RuOH]^{3+}$	3/2	2.08	2.09	1.36	1.36	1.89	1.43	6.34	1.50
$[A_3(o\text{-bpyOH})RuOH]^{3+}$	1/2	2.15	2.05	1.34	1.47	1.92	1.41	2.87	NA
$[A_3(m\text{-bpyOH})RuOH]^{3+}$	1/2	2.17	2.12	1.34	1.31	1.93	1.39	4.83	1.49
$[A_3(p\text{-bpyOH})RuOH]^{3+}$	1/2	2.17	2.11	1.34	1.39	1.93	1.29	6.54	1.45

[a] The C* atom indicates the carbon to which OH has added on the bpy ligand, while $\langle r_{C-C^*}\rangle$ is the average C−C bond distance between C* and its nearest neighbors. S indicates the overall spin state of the complex. A = NH_3.

arrangements may be imagined: the high-spin $S = 5/2$, two $S = 3/2$, and two $S = 1/2$ states. Of these, only the intermediate-spin and low-spin states on the metal center need be considered, leaving $S = 3/2$ and $1/2$ states (those relevant to this study are presented in Figure 1). Water addition to the bpy ligand of the $S = 1$ states of $[(NH_3)_3(bpy)Ru{=}O]^{2+}$ and $[(NH_3)_3(bpy)RuOH]^{3+}$ results in $S = 1$ and 0 potential spin products. Each of these products were similarly optimized for addition at the ortho (atomic label C_a in Figure 1), meta (C_b), and para (C_c) positions. Normal mode analysis confirmed each species to be a local minimum with no imaginary vibrations. In cases of open-shell singlet and doublet states, the broken-symmetry broken-spin methodology was used.[23] Complementary calculations were performed on $Ru(bpy)_3^{n+}$ ($n = 3-5$) so as to yield further insight into the electronic structure of the monomeric model catalysts.

To evaluate the thermodynamics of water addition, the gas-phase electronic energies, enthalpies, and free energies were examined. The free energies in solution were obtained through single-point calculations using a polarizable continuum model (PCM) with cavities generated by the united atom method.[24] While the importance of explicit solvation has been recently pointed out,[15] it is likely that extended H-bonding networks caused by the first solvation shell will have the largest impact upon the activation barriers for H_2O addition. This work focuses upon the net thermodynamic features of the covalent hydration reactions, and thus, only a PCM has been used. The solvent-corrected free energies of reactions a−c in Figure 1 are defined by

$$\Delta G_{corr} = \Delta G^{298} + \Delta\Delta G_{solv}^{tot} + SS_{corr}$$

which has ΔG_{298} as the free energy of the reaction in the gas phase, $\Delta\Delta G_{solv}^{tot}$ as the solvation contribution to the free energy of the reaction, and SS_{corr} as the standard-state thermodynamic correction (−4.3 kcal/mol for the single H_2O reactant).[25]

The electronic structures of the reactants and products, as well as $Ru(bpy)_3^{5+-3+}$, were analyzed using natural population analysis (NPA), obtained with the NBO program[26,27] (version 3.1) implemented in Gaussian03.[28] Spin densities were analyzed using both Mulliken and NPA and found to be similar (see the Supporting Information). The electronic structure analysis was compared to EPR parameters (such as **g** and **A** tensors) that were calculated using the ORCA program package.[29] For calculation of g tensors, the gauge origin was set to the center of electronic charge (via keyword *ori* -3). Spin-unrestricted calculations with B3LYP and the Ahlrichs triple-ζ valence basis set with polarization, TZVP,[30] were employed at the optimized geometries described above. The isotropic g value, g_{iso}, is defined as one-third of the sum of the principal g values, and the **g**-tensor anisotropy, g_{aniso}, is defined as the difference between the largest and the smallest principal g value ($g_{max} - g_{min}$). The **g** matrix (**g**) is given as a sum of the free electron value (g_e) and **g** shift (Δ**g**), which represents the deviation from g_e

$$\mathbf{g} = g_e\mathbf{1} + \Delta\mathbf{g}$$

Here, the **g** shift (Δ**g**) consists of three contributions

$$\Delta\mathbf{g} = \Delta\mathbf{g}^{OZ/SOC} + \Delta\mathbf{g}^{RMC} + \Delta\mathbf{g}^{GC}$$

where the first term is the dominant contribution which arises in second-order perturbation theory as a cross term between the orbital Zeeman (OZ) and spin−orbit coupling operators (SOC).[31] This term is referred to as the paramagnetic orbital Zeeman/spin−orbit coupling cross term. The second and third terms, the relativistic mass correction and diamagnetic spin−orbit (or gauge correction) terms, are first-order contributions. The spin−orbit coupling (SOC) operator used in this work is an accurate mean-field (SOMF) approximation to the full Breit−Pauli spin−orbit operator.[32]

RESULTS AND DISCUSSION

To examine the thermodynamic constraints to covalent hydration of the bipyridine ligand within our model Ru water oxidation catalysts, reactions a, b, and c in Figure 1 have been examined (only the meridional isomer of the model monomeric catalysts is shown for clarity). In dimeric μ-oxo-bridged ruthenium ions with water-oxidizing capacity such as the "blue dimer", i.e., $[(bpy)_2Ru^{III}(OH_2)]_2O^{4+}$, one of the bipyridine ligands is in an equivalent position with one of the N atoms trans to the ruthenyl oxo atom. The other bipyridine in the dimer is chelated with both N atoms occupying positions cis to the oxo atom in a conformation approximated by the fac isomer of our model complex. In the study presented here, reactivity of the meridional isomer (whose bpy is trans to the ruthenyl oxo atom) is first reported. For those cases where the covalent hydration reaction is observed to be energetically favorable, the energetics of the fac isomer are then studied so that the reactivity of each of the bpy ligands present in $[Ru^{III}(bpy)_2(OH_2)]_2O^{4+}$ is examined.

Water Addition to $[(NH_3)_3(bpy)Ru{=}O]^{3+}$. In solution, monomeric Ru(V)−oxo catalysts such as $[(tpy)(bpm)Ru^{V}O]^{3+}$ and $[(tpy)(bpz)Ru^{V}O]^{3+}$ are obtained by Ce(IV) oxidation under acidic conditions.[16] The optimized structure of *mer*-$[(NH_3)_3(bpy)Ru{=}O)]^{3+}$ (Table 1) is very similar to published DFT structures of both mononuclear catalysts and the Ru "blue dimer".[14,16,17] Using the atomic numbering presented in Figure 1, the ruthenyl bond length, r_{Ru-O_a}, is 1.77 Å and a trans effect is observed such that $r_{Ru-N_a'}$ is 0.17 Å longer than r_{Ru-N_a}. A similar trans effect was also observed in the DFT structure of $[(bpy)_2Ru^{V}O]_2O^{4+}$.[14] Although the Ru is formally in the +5 oxidation state (d^3), both NPA and Mulliken population analyses predict that the formal O^{2-} ligand donates nearly two electrons to the empty Ru d orbitals and the bpy ligand is electron deficient by 1.5 electrons, such that Ru has a d occupation of ~6.5. This leads to a very interesting distribution of unpaired spin density,

dx.doi.org/10.1021/ic200646h |*Inorg. Chem.* 2011, 50, 8177–8187

Table 2. Calculated Spin Densities (using NPA) and *g* Tensors for the Reactant, $[A_3(bpy)Ru{=}O]^{3+}$ (where A = NH_3), and Products of Reaction a Illustrated in Figure 1[a]

spin density	*S*	Ru	O_a	$(NH_3)_3$	bpy	O_b
$[A_3(bpy)Ru{=}O]^{3+}$	3/2	1.00	1.11	0.00	0.90	NA
$[A_3(o\text{-bpyOH})RuOH]^{3+}$	3/2	1.39	0.57	−0.02	1.02	0.05
$[A_3(m\text{-bpyOH})RuOH]^{3+}$	3/2	1.40	0.52	−0.02	1.06	0.04
$[A_3(p\text{-bpyOH})RuOH]^{3+}$	3/2	1.34	0.49	−0.02	1.12	0.07
$[A_3(o\text{-bpyOH})RuOH]^{3+}$	1/2	0.88	0.36	−0.01	−0.22	0.00
$[A_3(m\text{-bpyOH})RuOH]^{3+}$	1/2	0.73	0.28	−0.01	0.01	0.00
$[A_3(p\text{-bpyOH})RuOH]^{3+}$	1/2	0.73	0.27	0.00	0.01	0.00
electronic **g**-tensors	*S*	g_{11}	g_{22}	g_{33}	g_{iso}	g_{aniso}
$[A_3(bpy)Ru{=}O]^{3+}$	3/2	2.006	2.023	2.028	2.019	0.022
$[A_3(o\text{-bpyOH})RuOH]^{3+}$	3/2	2.012	2.052	2.093	2.052	0.082
$[A_3(m\text{-bpyOH})RuOH]^{3+}$	3/2	2.013	2.054	2.093	2.053	0.081
$[A_3(p\text{-bpyOH})RuOH]^{3+}$	3/2	2.024	2.049	2.072	2.048	0.048
$[A_3(o\text{-bpyOH})RuOH]^{3+}$	1/2	2.084	2.135	2.270	2.163	0.186
$[A_3(m\text{-bpyOH})RuOH]^{3+}$	1/2	1.977	2.173	2.360	2.170	0.383
$[A_3(p\text{-bpyOH})RuOH]^{3+}$	1/2	1.970	2.189	2.376	2.178	0.406

[a] *S* indicates the overall spin state of the complex where g_e = 2.002319, $g_{iso} = (g_{11} + g_{22} + g_{33})/3$, $g_{aniso} = g_{max} - g_{min}$.

with approximately one electron each on the ruthenium, ruthenyl−oxygen, and the bpy ligand (Table 2). The lone electron on bpy is delocalized almost symmetrically over the two rings of the ligand as observed in the singly occupied ligand-based Löwdin natural orbital shown in Figure 2 and the calculated atomic spin densities which indicate distribution over the $C_b(C_b')$, $C_d(C_d')$, and $C_e(C_e')$ atoms (Table S1 in the Supporting Information). This electronic structure is very similar to that observed in complementary calculations on *S* = 3/2 $Ru(bpy)_3^{5+}$, wherein the Löwdin spin densities indicate that ∼1.5 lone electrons are delocalized across the three bpy ligands. EPR calculations on $[(NH_3)_3(bpy)Ru{=}O]^{3+}$ indicate that the principal *g* values are all above the free electron *g* value, g_e (=2.002319) (Table 2). The departure of g_{iso} from g_e, known as the isotropic **g**-shift, is ∼0.02. The dominant contribution to this shift comes from the metal atom (∼84%), with a small contribution from metal-bound oxygen atom (∼13%) (Table S2 in the Supporting Information). Interestingly, the contribution to the **g** shift from the bpy ligand is negligible. These observations can be rationalized by considering the significantly larger spin−orbit (SO) coupling constant of the metal (Ru) compared to the small SO coupling constant of the light ligand atoms. The simulated spectrum of this complex shows a near axial EPR signal with a small **g**-tensor anisotropy of 0.022 (Figure S1 in the Supporting Information). While these **g**-tensor calculations are not expected to have quantitative accuracy due to limitations associated with the existing density functionals and basis sets, use of the hybrid B3LYP functional has been previously shown to yield good agreement with experimental data for transition-metal complexes.[33,34] Given the treatment of the SOC operator by an accurate mean-field approximation to the full Breit−Pauli spin−orbit operator, these EPR calculations should provide significant qualitative insights into the trends of the **g**-tensors of the monomeric Ru catalysts studied in this work.

The thermodynamics of water addition via reaction a in Figure 1 to form ortho, meta, or para products in either the 3/2 or the 1/2 spin states were calculated. Considering first the

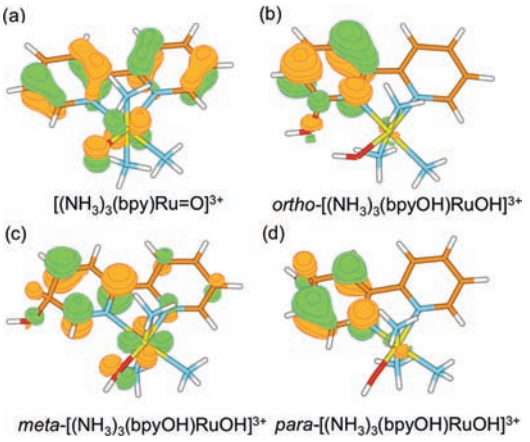

Figure 2. Singly occupied ligand-based Löwdin natural orbitals for (a) $[(NH_3)_3(bpy)Ru{=}O]^{3+}$ (*S* = 3/2), (b) *o*-$[(NH_3)_3(bpyOH)RuOH]^{3+}$ (*S* = 3/2), (c) *m*-$[(NH_3)_3(bpyOH)RuOH]^{3+}$ (*S* = 3/2), and (d) *p*-$[(NH_3)_3(bpyOH)RuOH]^{3+}$ (*S* = 3/2).

3/2 states of the three isomers, it is observed that water addition to the Ru=O, forming Ru−OH, serves to lengthen the metal−oxygen bond by ∼0.1 Å, the Ru−N_a' bond, $r_{Ru\text{-}N_a'}$, is shortened by ∼0.2 Å, and the Ru−N_a bond, r_{Ru-N_a}, is slightly shortened by 0.01 Å (Table 1). Upon formation of the addition product, $r_{C_a-N_a}$ is lengthened by 0.14 Å for the ortho isomer. Severe disruptions in the π-bonding framework of the bpy are observed due to changes in hybridization of the newly formed −HCOH− unit in the ligand ring. Here, the C−N bond, $r_{C_a-N_a}$, is 0.1 Å longer than $r_{C_a'-N_a'}$ for the ortho product (Figure 1) and the *o*-carbon to which the OH has been added is tilted below the plane of the ligand ring. Similar observations are observed for the meta and para products (see the Supporting Information).

From an electronic structure perspective, NPA predicts that the formal reduction caused by water addition leads to only ∼0.3 electrons gained by the $(NH_3)_3(bpy)Ru{=}O$ unit, most of which goes to the ruthenyl oxo atom and bpy ligand while the Ru becomes more electron deficient by 0.2 electrons. For all three *S* = 3/2 $[(NH_3)_3(bpyOH)RuOH]^{3+}$ products (ortho, meta, and para), 1.3−1.4 unpaired electrons are localized on ruthenium while ∼0.5 e^- are delocalized to the oxo group (Table 2). The spin density on the bpy ligand slightly increases but still may be considered a radical. As opposed to the reactant, most of the unpaired electron density is distributed over the pyridine ring containing the C atom to which OH has added. There the lone electron is distributed through the atoms C_a-C_e with alternating signs. The spin density on N_a was found to be negative in the meta isomer, in contrast to the ortho and para products (Table S3 in the Supporting Information). The unpaired spin density is distributed mostly over the N_a, C_b, and C_d atoms in ortho and para products, while it is distributed over the atoms C_a, C_c, and C_e in the meta isomer, as observed in the singly occupied ligand-based Löwdin natural orbitals shown in Figure 2. The spin densities on the *o*-, *m*-, and *p*-C atoms are fairly small.

EPR calculations show that the isotropic *g* values, g_{iso}, deviate significantly (0.05−0.18) from that of the free electron in all ruthenium products studied (Table 2). This can be attributed mostly to the large spin−orbit coupling constant of Ru, as the dominant contribution to the **g**-shifts stems from the paramagnetic orbital Zeeman/spin−orbit coupling cross term.[31,33,35] The isotropic **g**-shifts of spin 3/2 products are ∼0.030 larger

dx.doi.org/10.1021/ic200646h |*Inorg. Chem.* 2011, 50, 8177–8187

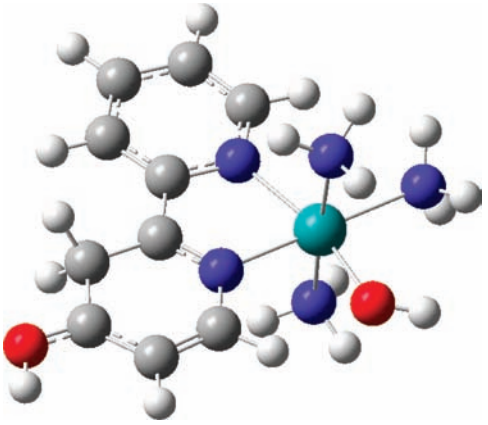

Figure 3. B3LYP/LANL2DZ/aug-cc-pVDZ-optimized geometry of the tautomerized *p*-$[(NH_3)_3(bpyOH)RuOH]^{3+}$ "covalent hydration" product ($S = 1/2$ state).

than that of the reactant (Table 2). The dominant contribution to the **g**-shifts stems from the metal atom, whereas the metal-bound oxygen and bpy ligand contribute negligibly (Table S4 in the Supporting Information). This is consistent with the shift in spin density from metal-bound oxygen to the metal for the spin 3/2 products. The **g**-tensor anisotropies of spin 3/2 products are ~0.03−0.06 larger than that of the reactant, $[(NH_3)_3(bpy)Ru{=}O]^{3+}$, as shown in Figures S1-a and S1-b in the Supporting Information. The increase in the **g**-tensor anisotropy is consistent with the increased spin density on the metal (from 1.0 to 1.3−1.4, Table 2). For the $[(NH_3)_3(bpyOH)RuOH]^{3+}$ products with $S = 3/2$, the departure of the isotropic g value from g_e is the smallest (0.046) in the para isomer as is the **g**-tensor anisotropy, g_{aniso} (0.048, Table 2). This is expected given that the unpaired spin density on the Ru center is smallest for the para isomer when $S = 3/2$.

Figure 1 presents three of the $S = 1/2$ states that can be produced from water addition reaction a to the bpy ligand. The lowest energy $S = 1/2$ state is found to be closed shell on the bpyOH ligand and $S = 1/2$ on the Ru center, forming effectively a ligand π cation bound to the reduced metal center ($\langle S^2 \rangle$ = ~0.75, Tables S6 and S7 in the Supporting Information). A second $S = 1/2$ state, higher in energy, was found with $\langle S^2 \rangle = 1.5-1.7$ (depending on the product isomer) that is an open-shell doublet where a bpyOH ligand radical is coupled antiferromagnetically to the $S = 1$ Ru metal center (energies presented in Table S6 in the Supporting Information). A third and final $S = 1/2$ was attempted that pairs the four Ru d electrons as $S = 0$, leaving the $S = 1/2$ bpyOH ligand radical; however, all of the calculations performed converged to the ground state. Geometry optimization of the ortho, meta, and para $S = 1/2$ isomers was initiated from the optimized $S = 3/2$ structures. While the ortho and meta $S = 1/2$ products have similar geometries to their 3/2 counterparts, the −HCOH− unit of the ligand ring in the para isomer rearranges and an H atom is transferred to the neighboring −CH− group, resulting in a ring structure characterized by $-COHCH_2-$ (Figure 3). It is further observed that the Ru−OH bond of all product isomers, r_{Ru-OH}, is ~0.05 Å longer than in the $S = 3/2$ state. The Ru−N_a' bond, $r_{Ru-N_a'}$, is also longer by 0.03−0.1 Å (Table 1). The unpaired spin density is mostly located on ruthenium (~75%) and oxygen O_a (~25%) (Table 2), with essentially no spin density on the bpy ligand. As such, EPR yields rhombic spectra; the meta and para isomers display two principal g values larger than g_e and one g value smaller than g_e (Figure S1 in the Supporting Information), which is in agreement with typical spectra of low-spin $4d^5$ ($S = 1/2$) distorted octahedral mononuclear ruthenium(III) complexes.[36−39] In the ortho isomer, all the **g**-shifts are positive in sign and the metal contribution is dominant (Table S9 in the Supporting Information). The distribution of unpaired spin over the metal d orbitals in the ortho isomer differs from the other two isomers such that spin density is primarily located in the d_{xz} orbital in meta and para isomers while it is distributed between d_{yz} and d_{xz} (slightly larger on d_{yz}) in the ortho isomer (Table S11 in the Supporting Information). Moreover, the spin density on d_{z2} and d_{x2-y2} orbitals is larger in the ortho isomer than the other two isomers. The observed **g**-tensor is attributed to these differences in the spin populations within the metal d orbitals in the ortho isomer.

To place these results in context, the X-band EPR measurements of ruthenium complexes with redox-active quinonoid ligands, in particular cationic complexes $[Ru(acac)_2(L)]^+$ (L = redox-active *o*-quinonoid ligand), have shown two g components larger than g_e and one smaller than g_e with **g**-tensor anisotropies of ~0.2−0.3. These properties lead to the assignment of these complexes as predominantly $Ru^{III}(d^5)-L^{0}$.[40] A later DFT study on these cationic complexes confirmed this assignment, based upon spin density analyses which predicted dominant spin density on the metal.[33] Thus, the large **g**-tensor anisotropies found in this work for the $S = 1/2$ products are indicative of the dominant metal contribution to the singly occupied orbital and consistent with their electronic structure. The isotropic **g**-shift of the $S = 1/2$ products increases by ~0.12 relative to that of the $S = 3/2$ products (Table 2). The **g**-tensor anisotropies are significantly larger for $[(NH_3)_3(bpyOH)RuOH]^{3+}$ products with $S = 1/2$ (Table 2) relative to the 3/2 state, as observed by comparing Figures S1-b and S1-c in the Supporting Information. Thus, our EPR calculations predict distinctive EPR signatures for the "covalent hydration" products as a function of both the position of OH addition to bipyridine and the overall spin state of the complex.

In the gas phase, addition to form a 3/2 product is enthalpically favored only for solvent attack at C_a (ortho position) (Table 3). The gas-phase free energies for water addition are all unfavored, which indicates that a single water molecule does not accurately reflect the entropy of water within the bulk. Addition of a polarizable continuum model (PCM) does not address the issue of entropy; however, it does take into account the significant effect of the bulk dielectric upon the highly charged reactants and products. In solution, only production of the meta product may be considered favorable ($\Delta G_{corr} = -0.50$ kcal/mol) (Table 3); however, this is within the error of the calculation (at this level of theory), and it is more likely that this is a thermoneutral process. Interestingly, formation of the "covalent hydration" products in the closed-shell low-spin $S = 1/2$ states is significantly more favorable than in the 3/2 states. Reaction to form the $S = 1/2$ species is predicted to be characterized by negative energies, enthalpies, and free energies of reaction (Table 3). Within the PCM, addition to form the meta product is the most favored ($\Delta G_{corr} = -16.30$ kcal/mol) whereas formation of the para product is the least favored ($\Delta G_{corr} = -0.99$ kcal/mol) (Table 3). This indicates that the overall favorability of the "covalent hydration" reaction is highly sensitive to both the overall spin state of the complex as well as the position of the OH attack.

dx.doi.org/10.1021/ic200646h |*Inorg. Chem.* 2011, 50, 8177–8187

Table 3. B3LYP/LANL2DZ/aug-cc-pVDZ Gas-Phase Thermodynamic Values (ΔE_{ZPE}^{298}, ΔH^{298}, ΔG^{298}), Free Energy Correction $\Delta\Delta G_{solv}$(tot) in Solution, and Final Solution-Phase Free Energy of Reaction ΔG_{corr} (using a standard state correction of −4.3 kcal/mol) for Reactions a−c in Figure 1 (in units of kcal/mol)[a]

reactant	product	S	ΔE_{ZPE}^{298}	ΔH^{298}	ΔG^{298}	$\Delta\Delta G_{solv}$(tot)	ΔG_{corr}
$[A_3(bpy)Ru{=}O]^{3+}$	$[A_3(o\text{-bpyOH})RuOH]^{3+}$	3/2	−5.67	−6.27	6.06	−0.04	1.72
	$[A_3(m\text{-bpyOH})RuOH]^{3+}$	3/2	1.20	0.60	9.95	−6.15	−0.50
	$[A_3(p\text{-bpyOH})RuOH]^{3+}$	3/2	4.60	4.01	13.55	−5.75	3.50
	$[A_3(o\text{-bpyOH})RuOH]^{3+}$	1/2	−14.69	−15.28	−4.99	1.78	−7.51
	$[A_3(m\text{-bpyOH})RuOH]^{3+}$	1/2	−21.55	−22.14	−14.17	2.17	−16.30
	$[A_3(p\text{-bpyOH})RuOH]^{3+}$	1/2	−51.79	−52.39	−3.04	6.35	−0.99
$[A_3(bpy)Ru{=}O]^{2+}$	$[A_3(o\text{-bpyOH})RuOH]^{2+}$	1	10.40	9.80	20.52	5.68	21.90
	$[A_3(m\text{-bpyOH})RuOH]^{2+}$	1	16.58	15.99	28.50	1.83	26.03
	$[A_3(p\text{-bpyOH})RuOH]^{2+}$	1	18.35	17.76	27.12	1.19	24.01
	$[A_3(o\text{-bpyOH})RuOH]^{2+}$	0	11.37	10.77	22.19	4.00	21.89
	$[A_3(m\text{-bpyOH})RuOH]^{2+}$	0	25.87	25.28	35.21	2.30	33.21
	$[A_3(p\text{-bpyOH})RuOH]^{2+}$	0	19.38	18.79	28.98	1.03	25.71
$[A_3(bpy)RuOH]^{3+}$	$[A_3(o\text{-bpyOH})RuOH_2]^{3+}$	1	−15.65	−16.24	−6.16	11.73	1.27
	$[A_3(m\text{-bpyOH})RuOH_2]^{3+}$	1	−5.01	−5.60	2.24	6.20	4.14
	$[A_3(p\text{-bpyOH})RuOH_2]^{3+}$	1	−1.81	−2.41	3.88	4.84	4.42
	$[A_3(o\text{-bpyOH})RuOH_2]^{3+}$	0	−18.33	−18.93	−10.07	14.04	−0.33
	$[A_3(m\text{-bpyOH})RuOH_2]^{3+}$	0	−17.56	−18.15	−11.35	15.50	−0.15
	$[A_3(p\text{-bpyOH})RuOH_2]^{3+}$	0	−13.07	−13.66	−6.26	10.39	−0.17

[a] The total spin is denoted by S and A = NH_3.

Table 4. B3LYP/LANL2DZ/aug-cc-pVDZ Gas-Phase Thermodynamic Values (ΔE_{ZPE}^{298}, ΔH^{298}, ΔG^{298}), Free Energy Correction $\Delta\Delta G_{solv}$(tot) in Solution, and Final Solution-Phase Free Energy of Reaction ΔG_{corr} (using a standard state correction of −4.3 kcal/mol) for Reaction a Using *fac*-$[(NH_3)_3(bpy)Ru{=}O]^{3+}$ as a reactant (in units of kcal/mol)[a]

reactant	product	S	ΔE_{ZPE}^{298}	ΔH^{298}	ΔG^{298}	$\Delta\Delta G_{solv}$(tot)	ΔG_{corr}
$[A_3(bpy)Ru{=}O]^{3+}$	$[A_3(o\text{-bpyOH})RuOH]^{3+}$	3/2	−11.65	−12.24	1.51	−0.87	−3.66
	$[A_3(m\text{-bpyOH})RuOH]^{3+}$	3/2	−2.89	−3.49	7.67	−6.56	−3.19
	$[A_3(p\text{-bpyOH})RuOH]^{3+}$	3/2	−23.78	−24.38	−10.90	−1.28	−16.48
	$[A_3(o\text{-bpyOH})RuOH]^{3+}$	1/2	−22.08	−22.67	−9.88	0.99	−13.19
	$[A_3(m\text{-bpyOH})RuOH]^{3+}$	1/2	−23.61	−24.2	−12.76	1.30	−15.76
	$[A_3(p\text{-bpyOH})RuOH]^{3+}$	1/2	−53.93	−54.52	−3.12	5.36	−2.06

[a] The total spin is denoted by S, and A = NH_3.

Given the energetic favorability of water addition to the *mer*-$[(NH_3)_3(bpy)Ru{=}O]^{3+}$, the reactivity of the facial isomer was also examined. The calculated molecular structure of *fac*-$[(NH_3)_3(bpy)Ru{=}O]^{3+}$ is in good agreement with the mer isomer (Table S13 in the Supporting Information). The ruthenyl bond length, r_{Ru-O_a}, is unchanged; however, unlike the meridional isomer, the Ru−N bond lengths are all identical. The electronic structure of the fac reactant is essentially the same as in the mer isomer, with approximately one electron each on the ruthenium, ruthenyl−oxygen, and bpy ligand (Table S14 in the Supporting Information). This necessarily leads to nearly identical EPR spectra as for the other isomer (Figure S1 in the Supporting Information). Addition of OH to the ortho, meta, and para positions of the bpy ligand in the facial isomer to produce products in the S = 3/2 or 1/2 state was also considered. As with the meridional isomer, water addition serves to lengthen the ruthenium−oxygen bond by ∼0.1 Å, and the Ru−N_a bond, r_{Ru-N_a}, was shortened by ∼0.1 Å (Table S13 in the Supporting Information). Upon formation of the addition product, the C_a−N_a bond, $r_{C_a-N_a}$, was lengthened by 0.14 Å for the ortho isomer and analogous distortions were observed in the meta and para isomers. As in the reactant, the electronic distribution of unpaired electron density for the water addition products was nearly identical to that of the meridional isomers (see the Supporting Information).

Interesting quantitative differences are observed in the gas- and solution-phase thermodynamics of the fac and mer isomers. First, unlike the reaction with the meridional isomer, addition to form the S = 3/2 product is energetically and enthalpically favored in the order para > ortho > meta (Table 4). The gas-phase free energy for water addition is only favored for solvent attack at the *p*-carbon of the bpy ligand. Within the PCM, addition to form the para product is the most favored (ΔG_{corr} = −16.48 kcal/mol) while formation of the meta product is the least favored (ΔG_{corr} = −3.19 kcal/mol). This is in contrast to the relative thermodynamics of formation of the meridional S = 3/2 products, where only the meta isomer was found to be energetically favorable. As in the reaction with the meridional isomer, formation of the S = 1/2 products for ortho and meta fac isomers is significantly more favorable than the S = 3/2 states. Formation of the S = 1/2 species is predicted to be characterized by negative energies, enthalpies, and free energies of reaction, as

dx.doi.org/10.1021/ic200646h |*Inorg. Chem.* 2011, 50, 8177–8187

Table 5. Key Bond Lengths (in Å) for Species in Reaction b Illustrated in Figure 1 As Calculated by B3LYP/LANL2DZ/aug-cc-pVDZ[a]

	S	$r_{Ru-N_a'}$	r_{Ru-N_a}	$r_{N_a'-C_a'}$	$r_{N_a-C_a}$	r_{Ru-O_a}	$r_{C^*-O_b}$	$r_{O_a-O_b}$	$\langle r_{C-C^*}\rangle$
$[A_3(bpy)Ru{=}O]^{2+}$	1	2.22	2.10	1.35	1.35	1.78	NA	NA	NA
$[A_3(o\text{-}bpyOH)RuOH]^{2+}$	1	2.14	2.07	1.35	1.47	1.94	1.45	2.99	NA
$[A_3(m\text{-}bpyOH)RuOH]^{2+}$	1	2.14	2.10	1.35	1.31	1.95	1.44	5.04	1.50
$[A_3(p\text{-}bpyOH)RuOH]^{2+}$	1	2.12	2.06	1.35	1.37	1.95	1.43	6.61	1.50
$[A_3(o\text{-}bpyOH)RuOH]^{2+}$	0	2.15	2.08	1.35	1.46	1.94	1.45	3.00	NA
$[A_3(m\text{-}bpyOH)RuOH]^{2+}$	0	2.02	2.11	1.36	1.30	1.99	1.42	5.26	1.50
$[A_3(p\text{-}bpyOH)RuOH]^{2+}$	0	2.12	2.07	1.35	1.37	1.95	1.43	6.64	1.50

[a] The C* atom indicates the carbon to which OH has added on the bpy ligand, while $\langle r_{C-C^*}\rangle$ is the average C−C bond distance between C* and its nearest neighbors. S indicates the overall spin state of the complex; A = NH_3.

Table 6. Calculated Spin Densities (using NPA) and *g* Tensors for the Meridional Reactant, $[(NH_3)_3(bpy)Ru{=}O]^{2+}$, and Products of Reaction b Illustrated in Figure 1[a]

spin density	S	Ru	O_a	$(NH_3)_3$	bpy	O_b
$[A_3(bpy)Ru{=}O]^{2+}$	1	0.93	1.07	0.00	0.01	NA
$[A_3(o\text{-}bpyOH)RuOH]^{2+}$	1	0.80	0.27	−0.01	0.90	0.05
$[A_3(m\text{-}bpyOH)RuOH]^{2+}$	1	0.76	0.26	−0.01	0.96	0.04
$[A_3(p\text{-}bpyOH)RuOH]^{2+}$	1	0.81	0.26	0.00	0.89	0.05
electronic g-tensors		g_{11}	g_{22}	g_{33}	g_{iso}[b]	g_{aniso}[c]
$[A_3(bpy)Ru{=}O]^{2+}$	1	2.006	2.031	2.039	2.025	0.034
$[A_3(o\text{-}bpyOH)RuOH]^{2+}$	1	1.998	2.095	2.182	2.092	0.184
$[A_3(m\text{-}bpyOH)RuOH]^{2+}$	1	1.994	2.109	2.226	2.109	0.232
$[A_3(p\text{-}bpyOH)RuOH]^{2+}$	1	1.992	2.086	2.181	2.086	0.189

[a] S indicates the overall spin state of the complex; A = NH_3. g_e = 2.002319. [b] $g_{iso} = (g_{11} + g_{22} + g_{33})/3$. [c] $g_{aniso} = g_{max.} - g_{min}$.

also observed for the meridional counterparts. Within the PCM, addition to form the para product is the least favorable (ΔG_{corr} = −2.06 kcal/mol) while formation of the meta product is the most favorable (ΔG_{corr} = −15.76 kcal/mol) (Table 4), consistent with the observations for meridional counterparts. Thus, comparison of water addition thermodynamics for the facial and meridional $[(NH_3)_3(bpy)Ru{=}O]^{3+}$ reactants indicate a slight preference for reactivity of the bpy ligand that coordinates cis to the ruthenyl oxo atom. For the facial isomer, water addition products in both the S = 3/2 and the S = 1/2 states are energetically favorable.

Water Addition to $[(NH_3)_3(bpy)Ru{=}O]^{2+}$. To fully examine the "covalent hydration" reaction as a function of Ru oxidation state, water addition to both the formal Ru(IV)=O and the Ru(IV)OH units has been studied. The geometry of *mer*-$[(NH_3)_3(bpy)Ru{=}O]^{2+}$ is nearly identical to that of the Ru(V) analogue, with bond distances generally within 0.02 Å of each other (Table 5). The exception is $r_{Ru-N_a'}$, which is trans to the Ru=O. In this instance a 0.07 Å contraction is observed relative to $[(NH_3)_3(bpy)Ru{=}O]^{3+}$, indicating a significantly smaller trans effect upon reduction of the complex ion. Comparison of the atomic electron populations on the three NH_3 ligands, bpy ligand, Ru, and ruthenyl oxo atom indicates that the added electron goes primarily to the bpy ligand, which was 1.5 e^- electron deficient in $[(NH_3)_3(bpy)Ru{=}O]^{3+}$, and the ruthenyl oxo atom. Within $[(NH_3)_3(bpy)Ru{=}O]^{2+}$, the total spin density is distributed evenly over ruthenium (0.93) and oxygen (1.07) (Table 6) and the spin density on the bpy ligand is negligible. Comparable calculations on $Ru(bpy)_3^{4+}$ indicate a similar trend (Tables S55 and S56 in the Supporting Information).

Water addition via reaction b in Figure 1 was considered, with production of ortho, meta, or para products in either the S = 1 or the S = 0 spin states. In both cases the formal reduction of the reactant occurs primarily at the ruthenyl oxo atom. For the three isomeric S = 1 $[(NH_3)_3(bpyOH)RuOH]^{2+}$ products, 0.8 unpaired electrons are located on ruthenium while 0.2−0.3 lone electrons are delocalized to the ruthenium-bound O atom (O_a) (Table 6). The bpy ligand radical has 0.9 unpaired electrons distributed over the pyridine ring containing the C atom to which OH is added. The spin density on N_a was found to be negative in the meta product, in contrast to the ortho and para products, and the density is distributed through the atoms C_a−C_e with alternating signs in all cases (Table S19 in the Supporting Information). The unpaired spin density is distributed mostly over the N_a, C_b, and C_d atoms in ortho and para products, while it is distributed over the atoms C_a, C_c, and C_e in the meta isomer. Water addition serves to lengthen the Ru−O bond, r_{Ru-O_a}, by ∼0.17 Å in all products with spin S = 1 (Table 5). The C_a−N_a bond, $r_{C_a-N_a}$, is also lengthened by ∼0.1 Å in the ortho isomer, similar to reaction a. In addition, it was observed that the Ru−N_a' bond, $r_{Ru-N_a'}$, is shortened by ∼0.1 Å for all isomers with the S = 1 state.

Three S = 0 states may result from OH addition to the bpy ligand (Figure 1). The first is an open-shell singlet, where the lone electron of the ligand radical is coupled antiferromagnetically to the S = 1/2 Ru metal center. Broken-spin broken-symmetry optimizations, except for the meta isomer, have converged to this state with $\langle S^2\rangle \approx 1.0$, with an overall energy higher than the S = 1 state (Table S6 in the Supporting Information). The second S = 0 state has a closed-shell electron configuration with the bpy ligand having two extra electrons in a closed-shell configuration, forming a π anion, and the Ru having four paired d electrons. The third S = 0 state has no extra electrons on the bpyOH ligand, now a π cation, and six paired Ru d electrons (Table S20 in the Supporting Information). Our calculations have converged to the third S = 0 state as the ground state of the meta isomer. In contrast, the open-shell singlet state (the first S = 0 state) was found to be lower in energy than the closed-shell singlet state for the ortho and para isomers (Table S6 in the Supporting Information). In the S = 0 geometries, the ortho and para isomers exhibit very similar structures to their S = 1 counterparts. For example, the Ru−N_a bond, r_{Ru-N_a}, and the Ru−N_a' bond, $r_{Ru-N_a'}$, are found to be only ∼0.01 Å longer for the ortho and para isomers compared with the S = 1 counterparts. Also, for these two isomers the Ru−O bond, r_{Ru-O_a}, is the same

dx.doi.org/10.1021/ic200646h |*Inorg. Chem.* 2011, 50, 8177–8187

Table 7. Key Bond Lengths (in Å) for Species in Reaction c Illustrated in Figure 1 As Calculated by B3LYP/LANL2DZ/aug-cc-pVDZ[a]

	S	$r_{Ru-N_a'}$	r_{Ru-N_a}	$r_{N_a'-C_a'}$	$r_{N_a-C_a}$	r_{Ru-O_a}	$r_{C^*-O_b}$	$r_{O_a-O_b}$	$\langle r_{C-C^*}\rangle$
$[A_3(bpy)RuOH]^{3+}$	1	2.11	2.05	1.35	1.36	1.94	NA	NA	NA
$[A_3(o\text{-}bpyOH)RuOH_2]^{3+}$	1	2.05	2.08	1.35	1.47	2.14	1.45	2.61	NA
$[A_3(m\text{-}bpyOH)RuOH_2]^{3+}$	1	2.05	2.06	1.35	1.32	2.28	1.43	5.05	1.50
$[A_3(p\text{-}bpyOH)RuOH_2]^{3+}$	1	2.02	2.08	1.36	1.37	2.20	1.43	6.47	1.50
$[A_3(o\text{-}bpyOH)RuOH_2]^{3+}$	0	2.07	2.00	1.35	1.48	2.22	1.42	2.67	NA
$[A_3(m\text{-}bpyOH)RuOH_2]^{3+}$	0	2.04	2.11	1.34	1.31	2.28	1.40	5.14	1.49
$[A_3(p\text{-}bpyOH)RuOH_2]^{3+}$	0	2.06	1.98	1.35	1.38	2.28	1.39	6.82	1.48

[a] The C* atom indicates the carbon to which OH has added on the bpy ligand, while $\langle r_{C-C^*}\rangle$ is the average C−C bond distance between C* and its nearest neighbors. S indicates the overall spin state of the complex; A = NH_3.

as that of corresponding isomers with S = 1 (Table 5), whereas for the S = 0 meta isomer, r_{Ru-O_a} is found to be 0.04 Å longer than that of the S = 1 meta isomer; the Ru−N_a' bond, $r_{Ru-N_a'}$, is ∼0.1 Å shorter than that of the S = 1 meta isomer (Table 5). Unlike the para-substituted S = 1/2 *mer*-$[(NH_3)_3(bpyOH)RuOH]^{3+}$ product (Figure 3), the geometries of all isomeric products conform to that shown in Figure 1, with no structural rearrangements. As in the water addition reaction to the Ru(V) reactant, the spin densities on the C atoms to which OH has added are fairly small. Note that the singlet closed-shell atomic spin densities are all zero, as expected for all three $[(NH_3)_3(bpyOH)RuOH]^{2+}$ products with spin S = 0.

EPR calculations show that the departure of g_{iso} from g_e, namely, the isotropic **g**-shift, is 0.023 for the reactant complex ion, $[(NH_3)_3(bpy)Ru{=}O]^{2+}$ (Table 6). The isotropic **g**-shift and g-tensor anisotropy become larger (∼0.07 and ∼0.17) for the products with spin S = 1 (Table 6). The EPR spectra of the S = 1 products are characterized by a rhombic **g**-tensor with two principal g values larger than g_e and one principal g value smaller than g_e. The products with the total spin S = 0 are EPR silent. In both the gas and the solution phases, water addition is not energetically favored, with positive energies, enthalpies, and free energies of reaction being observed irrespective of product spin state (Table 3). These results give further indication that the energetic favorability of the "covalent hydration" reaction is highly sensitive to the overall oxidation state of the Ru metal.

Water Addition to $[(NH_3)_3(bpy)RuOH]^{3+}$. The geometry of the $[(NH_3)_3(bpy)RuOH]^{3+}$ reactant is somewhat perturbed relative to both $[(NH_3)_3(bpy)Ru{=}O]^{2+}$ and the Ru(V) analogues. In addition to the anticipated lengthening of the metal−oxygen bond upon protonation, an increase in the N−C bond lengths is also observed (Table 7). Further, contraction of the Ru−N_a' bond length is observed such that $r_{Ru-N_a'}$ and r_{Ru-N_a} are within 0.05 Å of each other. Protonation of the ruthenyl oxo atom causes a shift in electron density from both ruthenium and bipyridine to the oxo atom, leading to enhanced unpaired spin density on the Ru center (∼76% of the total) and a decrease in unpaired electrons on the oxo atom (22% of the total) (Table 8).

Water addition via reaction c in Figure 1 was considered, with production of ortho, meta, or para products in either the S = 1 or the S = 0 spin states. Considering first the S = 1 products, it is observed that water addition serves to lengthen the Ru−O bond, r_{Ru-O_a}, by 0.1 Å in the ortho product and 0.2−0.3 Å in the meta and para products, respectively (Table 7). Upon formation of the addition product, the C−N bond, $r_{C_a-N_a}$, is lengthened by 0.1 Å

Table 8. Calculated Spin Densities (using NPA) and g Tensors for the Meridional Reactant, $[(NH_3)_3(bpy)RuOH]^{3+}$, and Products of Reaction c Illustrated in Figure 1[a]

spin density	S	Ru	O_a	$(NH_3)_3$	bpy	O_b
$[A_3(bpy)RuOH]^{3+}$	1	1.53	0.44	−0.03	0.06	NA
$[A_3(o\text{-}bpyOH)RuOH_2]^{3+}$	1	0.94	0.04	−0.01	0.99	0.04
$[A_3(m\text{-}bpyOH)RuOH_2]^{3+}$	1	0.95	0.00	0.00	1.00	0.06
$[A_3(p\text{-}bpyOH)RuOH_2]^{3+}$	1	0.92	0.03	−0.01	1.01	0.05
electronic g-tensors		g_{11}	g_{22}	g_{33}	g_{iso}[b]	g_{aniso}[c]
$[A_3(bpy)RuOH]^{3+}$	1	2.025	2.101	3.495	2.540	1.470
$[A_3(o\text{-}bpyOH)RuOH_2]^{3+}$	1	1.996	2.272	2.366	2.211	0.370
$[A_3(m\text{-}bpyOH)RuOH_2]^{3+}$	1	2.004	2.414	2.519	2.312	0.515
$[A_3(p\text{-}bpyOH)RuOH_2]^{3+}$	1	1.990	2.234	2.279	2.168	0.290

[a] S indicates the overall spin state of the complex; A = NH_3. g_e = 2.002319. [b] $g_{iso} = (g_{11} + g_{22} + g_{33})/3$. [c] $g_{aniso} = g_{max.} - g_{min}$.

in the ortho isomer. For the products of reaction c within the S = 1 state (Figure 1), the RuO unit gains ∼0.5 e^- relative to the reactant such that the total spin density is almost evenly distributed over the ruthenium and the bpy ligand, leaving essentially no spin density on O_a (Table 8). The unpaired spin density on the bpy ligand is distributed primarily over the pyridine ring containing the C atom to which OH is bound (Table S21 in the Supporting Information), with localization of spin density on N_a, C_b, and C_d for the ortho and para products and the unpaired electron mostly on C_a, C_c, and C_e for the meta product. Three S = 0 states may be produced in this reaction. The first is an open-shell state with the lone electron of the ligand radical antiferromagnetically coupled to the S = 1/2 Ru center (Table S6 in the Supporting Information). Two closed-shell S = 0 states can result from having (a) two paired electrons on the bpyOH, forming a π anion, and four paired d electrons on Ru or (b) six paired d electrons on the Ru center, leaving a π-cation ligand. Our calculations have resulted in the latter closed-shell state (Table S22 in the Supporting Information). Note that the singlet closed-shell atomic spin densities are all zero as expected for all three $[(NH_3)_3(bpyOH)RuOH_2]^{3+}$ products with spin S = 0. In general, the S = 0 geometries for the three isomers are quite similar to those found in the S = 1 states with the following exceptions: the Ru−O bond, r_{Ru-O_a}, is lengthened by 0.08 Å and r_{Ru-N_a} is shortened by ∼0.08−0.10 Å for the ortho and para isomers (Table 7).

EPR calculations predict a substantially larger isotropic **g**-shift (0.54) for $[(NH_3)_3(bpy)RuOH]^{3+}$ (Table 8) relative to the

dx.doi.org/10.1021/ic200646h |*Inorg. Chem.* 2011, 50, 8177–8187

other oxidation states of the reactants considered in this work. The significantly larger **g**-tensor anisotropy and the isotropic **g** shift can be rationalized by considering the substantial spin density (1.53) found on the ruthenium in $[(NH_3)_3(bpy)RuOH]^{3+}$. Unlike the reactant, the g_{iso} and **g**-tensor anisotropy values are much smaller for products with spin $S = 1$, where the spin density is delocalized between metal and the bpy ligand (Table 8). Although the total spin density is evenly distributed over the ruthenium and the bpy ligand, the dominant contribution to the **g** shift derives from the Ru with only a negligible contribution from the bpy ligand atoms (Table S24 in the Supporting Information). As such, the EPR spectrum is characterized by a rhombic *g* tensor with one principal *g* value smaller than that of the free electron value (except meta isomer) and two *g* values larger than g_e, in agreement with EPR spectra observed for low-spin d^5 ruthenium complexes.[36−39] The largest isotropic *g* value and also the largest **g**-tensor anisotropy were obtained for the meta product of reaction c in Figure 1 (Table 8), for which the unpaired spin density on Ru is also the largest (Table 8).

In the gas phase, addition to form the $S = 1$ products becomes energetically and enthalpically more favorable in the order ortho > meta > para (Table 3). However, the gas-phase free energy for water addition is only favored for solvent attack at the *o*-carbon of the bpy ligand (Table 3). Within the PCM, none of the $S = 1$ products are favored (Table 3). Formation of the closed-shell low-spin $S = 0$ states is more favorable than the $S = 1$ states. Here, all products have negative energies, enthalpies, and free energies of reaction (Table 3). Within the PCM, all of the $S = 0$ products are favored as opposed to the $S = 1$ products of reaction c in Figure 1.

RELEVANCE TO WATER OXIDATION CATALYSIS

The notion that bipyridine ligands in catalysts such as $Ru(bpy)_3^{3+}$ and the "blue dimer" might participate in water oxidation through formation of OH-substituted reaction transients has existed in the literature for some time.[4,10] However, to date, computational methods have not thoroughly examined the energetics of such a reaction pathway or the nature of the reaction products. In the present study, we confirm that "covalent hydration" with addition of OH to the bipyridine ring can be energetically favorable in our model compound under certain conditions but that the reaction thermodynamics are highly dependent upon the metal oxidation state, position of OH addition to the ring, and overall spin states of the reaction products (Tables 3 and 4). In general, this reaction is favorable for $[(NH_3)_3(bpy)Ru{=}O]^{3+}$ but not for $[(NH_3)_3(bpy)Ru{=}O]^{2+}$. Protonation of the oxo atom stabilizes the reaction product such that the reaction becomes nearly isoenergetic for $[(NH_3)_3(bpy)RuOH]^{3+}$. Both oxidation and protonation can be expected to decrease the electron density on the bpy ligand, thereby increasing its susceptibility to nucleophilic attack by an OH group. Addition to the ring meta position is generally energetically favored over the ortho and para positions for the $[(NH_3)_3(bpy)Ru{=}O]^{3+}$ reactant, the single exception being addition to the para position to form the $S = 3/2$ *fac*-$[(NH_3)_3(p\text{-bpyOH})RuOH]^{3+}$ product (Table 4). This pattern was not observed for $[(NH_3)_3(bpy)Ru{=}O]^{2+}$ and $[(NH_3)_3(bpy)RuOH]^{3+}$, where the energetically most favorable addition occurred at the *o*-carbon position. For reactions forming stable products, the driving force was generally greater for the lower total spin states, the single exception again being the *fac*-$[(NH_3)_3(p\text{-bpyOH})RuOH]^{3+}$ ($S = 3/2$) ion. In every case, the lowest energy electron configuration for these low-spin states are closed shell on the bpyOH ligand, which has become oxidized to a π cation by transfer of an electron to the Ru center. It is notable that for the Ru(V) isomeric ions, the "covalent hydrates" in the higher spin states that contain neutral bpyOH ligand radicals are also isoenergetic with or more stable than the reactants. Another general trend evident from the data in Tables 3 and 4 is the greater stabilities of the Ru(V) facial isomers, which may arise from a strong trans effect of the coordinated oxo atom, leading to relative destabilization of bipyridine in the corresponding meridionally-bound isomers.

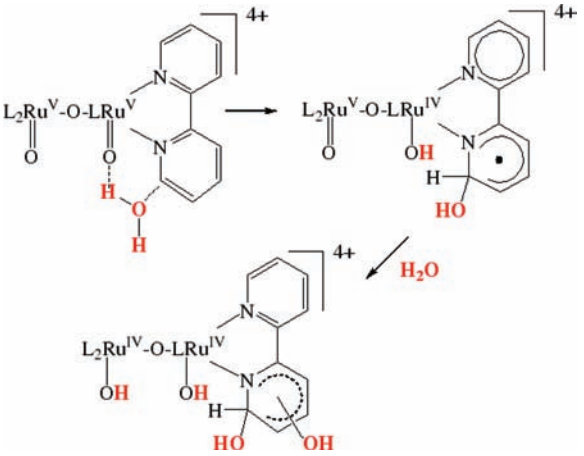

Figure 4. "Covalent hydration" reactions of the "blue dimer". The first two steps of a proposed pathway for O_2 formation from two solvent molecules are shown. In step 1, H-atom abstraction by a ruthenyl oxo group is accompanied by concerted addition of the OH fragment to the proximate bipyridine ring, forming a ligand radical intermediate. In step 2, subsequent internal electron transfer is accompanied by addition of a second water molecule, forming a diol. In this step, water addition need not be concerted. L = 2,2′-bipyridine. Atoms derived from solvent are indicated in red. Adapted from ref 10.

Our model complexes differ significantly from monomeric ruthenium water oxidation catalysts such as $[(tpy)(bpm)Ru{=}O]^{2+/3+}$ and $[(tpy)(bpz)Ru{=}O]^{2+/3+}$ in that ligands capable of π-backbonding have been replaced by strongly σ-donating ammine ligands, which are expected to destabilize the coordinated bipyridine toward nucleophilic attack. In this sense, the model complexes might better represent the electronic structure of the "blue dimer", in which the oxo-bridging fragment $\{-O-Ru^{III}(OH_2)(bpy)_2^{2+}\}$ also acts as a strong σ donor to the second Ru center.[41,42] One remarkable feature of the calculations is that the most stable adducts are often species in which internal electron transfer has occurred, effectively generating a one-electron oxidized ligand π cation coordinated to a reduced (d^5 or d^6) Ru atom (Figure 1). These internal electronic rearrangements are reminiscent of bimolecular reactions between free and Ru-complexed bpyOH radical adducts and weak oxidants which have been proposed from studies involving radiolytically generated $OH^{\bullet}$ radicals.[43] In these latter studies, the oxidized $bpyOH^+$ π cation appears to undergo rapid addition of hydroxide ion to produce a ring-substituted diol. This chemistry has provided experimental support for our hypothesis that the "blue dimer" can form similar species following "covalent hydration" of one of its bipyridine ligands en route to net water oxidation. The first few steps of a possible mechanism for this reaction are reproduced in Figure 4. In any event, these considerations suggest a

dx.doi.org/10.1021/ic200646h |*Inorg. Chem.* 2011, 50, 8177–8187

second remarkable feature of the calculations, namely, that despite forming reactive molecules as immediate products, "covalent hydration" reactions involving the Ru^{V}=O and Ru^{IV}−OH model complexes are thermodynamically favorable. Although this aspect has not been explored in the present studies, these products are also expected to add a second water molecule to generate more stable ring-substituted diols. A third remarkable feature of these reactions is that the electron density on the metal center does not change appreciably upon oxidation to Ru(V). Indeed, the calculations show that net oxidation involves removal of electron density primarily from the bipyridine ligand, i.e., net oxidation of the ligand. This behavior is reminiscent of results obtained from DFT analyses of the so-called "Tanaka catalyst",[44] where $4e^-$ cycling of the dinuclear Ru complex to electrocatalytically oxidize water involves net changes in apparent oxidation state within noninnocent peripheral ligands, while the operational oxidation state of Ru remains essentially unchanged.

Possible addition of OH to the pyridine ring trans to the Ru=O bond (in the meridional isomer) has not been considered in this study. The likelihood of this occurring seems remote based upon energetic and spatial constraints associated with water addition. Specifically, there is insufficient driving force to generate free $OH^{\bullet}$ as a reaction intermediate, so that water addition must be a concerted process.[12a] The relatively large distance between the ruthenyl oxo atom and the $C_a'-C_c'$ atoms of the trans-coordinated ring therefore preclude this from happening without encountering a large activation barrier. Ongoing studies are being directed at analyzing activation barriers for the various covalent hydrates and potential channels for their secondary decay to further species.

■ ASSOCIATED CONTENT

Supporting Information. This material is available free of charge via the Internet at http://pubs.acs.org.

■ AUTHOR INFORMATION

Corresponding Authors

*E-mail: abdullah.ozkanlar@wsu.edu (A.O.); auclark@wsu.edu (A.E.C.).

■ ACKNOWLEDGMENT

The authors are grateful to David Britt and members of his research group at the University of California at Davis, particularly Stefan Stoll, Troy Stich, and Jamie Stull, for helpful discussions concerning the simulation and interpretation of EPR spectra. This research was performed using the Molecular Science Computing Facility (MSCF) at the William R. Wiley Environmental Molecular Sciences Laboratory, a national scientific user facility sponsored by the U.S. Department of Energy's Office of Biological and Environmental Research located at the Pacific Northwest National Laboratory, operated for the Department of Energy by Battelle. Research in the authors' laboratories is funded by the Division of Chemical Sciences, Geosciences, and Biosciences, Office of Basic Energy Sciences of the U.S. Department of Energy, through Grant DE-FG02-06ER15820.

■ REFERENCES

(1) (a) Gillard, R. D. *Coord. Chem. Rev.* **1975**, *16*, 67–94. (b) Gillard, R. D. *Coord. Chem. Rev.* **1983**, *50*, 303.

(2) (a) Albert, A.; Armarego, W. L. F. *Adv. Heterocycl. Chem.* **1965**, *4*, 1–42. (b) Perrin, D. D. *Adv. Heterocycl. Chem.* **1965**, *4*, 43–73. (c) Albert, A. *Adv. Heterocycl. Chem.* **1976**, *20*, 117.

(3) Serpone, N.; Ponterini, G.; Jamieson, M. A.; Bolletta, F.; Maestri, M. *Coord. Chem. Rev.* **1983**, *50*, 209.

(4) Creutz, C.; Sutin, N. *Proc. Natl. Acad. Sci. U.S.A.* **1975**, *72*, 2858.

(5) Hurst, J. K. *Coord. Chem. Rev.* **2005**, *249*, 313.

(6) Ghosh, P. K.; Brunschwig, B. S.; Chou, M.; Creutz, C; Sutin, N. *J. Am. Chem. Soc.* **1984**, *106*, 4772.

(7) Ledney, M.; Dutta, P. *J. Am. Chem. Soc.* **1995**, *117*, 7687.

(8) Yamada, H.; Siems, W. F.; Koike, T.; Hurst, J. K. *J. Am. Chem. Soc.* **2004**, *126*, 9786.

(9) Cape, J. L.; Siems, W. F.; Hurst, J. K. *Inorg. Chem.* **2009**, *48*, 8729.

(10) Hurst, J. K.; Cape, J. L.; Clark, A. E.; Das, S.; Qin, C. *Inorg. Chem.* **2008**, *47*, 1753.

(11) Liu, F; Concepcion, J. J.; Jurss, J. W.; Cardolaccia, T.; Templeton, J. L.; Meyer, T. *J. Inorg. Chem.* **2008**, *47*, 1727.

(12) (a) Yamada, H.; Hurst, J. K. *J. Am. Chem. Soc.* **2000**, *122*, 5303. (b) Cape, L. J.; Hurst, J. K. *J. Am. Chem. Soc.* **2008**, *130*, 827.

(13) Lymar, S. Unpublished observations.

(14) Yang, X.; Baik, M.-H. *J. Am. Chem. Soc.* **2006**, *128*, 7476.

(15) Wang, L.-P.; Wu, Q.; Van Voorhis, T. *Inorg. Chem.* **2010**, *49*, 4543.

(16) Concepcion, J. J.; Jurss, J. W.; Templeton, J. L.; Meyer, T. J. *J. Am. Chem. Soc.* **2008**, *130*, 16462.

(17) Concepcion, J. J.; Tsai, M.-K.; Muckerman, J. T.; Meyer, T. J. *J. Am. Chem. Soc.* **2010**, *132*, 1545.

(18) Clark, A. E.; Hurst, J. K. *Prog. Inorg. Chem.* **2010**in press.

(19) (a) Becke, A. D. *J. Chem. Phys.* **1993**, *98*, 5648.

(20) (a) Hay, P. J.; Wadt, W. R. *J. Chem. Phys.* **1985**, *82*, 270. (b) Hay, P. J.; Wadt, W. R. *J. Chem. Phys.* **1985**, *82*, 284. (c) Hay, P. J.; Wadt, W. R. *J. Chem. Phys.* **1985**, *82*, 299.

(21) Dunning, T. H., Jr. *J. Chem. Phys.* **1989**, *90*, 1007.

(22) Bylaska, E. J.; de Jong, W. A.; Kowalski, K.; Straatsma, T. P.; Valiev, M.; Wang, D.; Aprà, E.; Windus, T. L.; Hirata, S.; Hackler, M. T.; Zhao, Y.; Fan, P.-D.; Harrison, R. J.; Dupuis, M.; Smith, D. M. A.; Nieplocha, J.; Tipparaju, V.; Krishnan, M.; Auer, A. A.; Nooijen, M.; Brown, E.; Cisneros, G.; Fann, G. I.; Früchtl, H.; Garza, J.; Hirao, K.; Kendall, R.; Nichols, J. A.; Tsemekhman, K.; Wolinski, K.; Anchell, J.; Bernholdt, D.; Borowski, P.; Clark, T.; Clerc, D.; Dachsel, H.; Deegan, M.; Dyall, K.; Elwood, D.; Glendening, E.; Gutowski, M.; Hess, A.; Jaffe, J.; Johnson, B.; Ju, J.; Kobayashi, R.; Kutteh, R.; Lin, Z.; Littlefield, R.; Long, X.; Meng, B.; Nakajima, T.; Niu, S.; Pollack, L.; Rosing, M.; Sandrone, G.; Stave, M.; Taylor, H.; Thomas, G.; Wong, A.; Zhang, Z.; NWChem, A Computational Chemistry Package for Parallel Computers, Version 5.1, Pacific Northwest National Laboratory, Richland, WA, 99352-0999, USA, 2007.

(23) (a) Noodleman, L. J. *Chem. Phys.* **1981**, *74*, 5737. (b) Noodleman, L.; Davidson, E. R. *Chem. Phys.* **1986**, *109*, 131.

(24) (a) Mennucci, B.; Tomasi, J. *J. Chem. Phys.* **1997**, *106*, 5151. (b) Mennucci, B.; Cances, E.; Tomasi, J. *J. Phys. Chem. B* **1997**, *101*, 10506.

(25) Asthagiri, D.; Pratt, L. R.; Ashbaugh, H. S. *J. Chem. Phys.* **2003**, *119*, 2702–2708.

(26) Foster, J. P.; Weinhold, F. *J. Am. Chem. Soc.* **1980**, *102*, 7211.

(27) Reed, A. E.; Weinstock, R. B.; Weinhold, F. *J. Chem. Phys.* **1985**, *83*, 735.

(28) Frisch, M. J.; Trucks, G. W.; Schlegel, H. B.; Scuseria, G. E.; Robb, M. A.; Cheeseman, J. R.; Montgomery, Jr., J. A.; Vreven, T.; Kudin, K. N.; Burant, J. C.; Millam, J. M.; Iyengar, S. S.; Tomasi, J.; Barone, V.; Mennucci, B.; Cossi, M.; Scalmani, G.; Rega, N.; Petersson, G. A.; Nakatsuji, H.; Hada, M.; Ehara, M.; Toyota, K.; Fukuda, R.; Hasegawa, J.; Ishida, M.; Nakajima, T.; Honda, Y.; Kitao, O.; Nakai, H.; Klene, M.; Li, X.; Knox, J. E.; Hratchian, H. P.; Cross, J. B.; Bakken, V.; Adamo, C.; Jaramillo, J.; Gomperts, R.; Stratmann, R. E.; Yazyev, O.; Austin, A. J.; Cammi, R.; Pomelli, C.; Ochterski, J. W.; Ayala, P. Y.; Morokuma, K.; Voth, G. A.; Salvador, P.; Dannenberg, J. J.; Zakrzewski, V. G.; Dapprich, S.; Daniels, A. D.; Strain, M. C.; Farkas, O.; Malick, D. K.; Rabuck, A. D.; Raghavachari, K.; Foresman, J. B.; Ortiz, J. V.; Cui, Q.; Baboul, A. G.; Clifford, S.; Cioslowski, J.; Stefanov, B. B.; Liu, G.;

Liashenko, A.; Piskorz, P.; Komaromi, I.; Martin, R. L.; Fox, D. J.; Keith, T.; Al-Laham, M. A.; Peng, C. Y.; Nanayakkara, A.; Challacombe, M.; Gill, P. M. W.; Johnson, B.; Chen, W.; Wong, M. W.; Gonzalez, C.; Pople, J. A. *Gaussian 03*, Revision E.01; Gaussian, Inc.: Wallingford, CT, 2004.

(29) (a) Neese, F. *ORCA*, Version 2.7; Institute for Physical and Theoretical Chemistry; University of Bonn: Bonn, Germany, 2010. (b) Lee, C.; Parr, R. G.; Yang, W. *Phys. Rev. B* **1988**, *37*, 785.

(30) (a) Schaefer, A.; Horn, H.; Ahlrichs, R. *J. Chem. Phys.* **1992**, *97*, 2571. (b) Ahlrichs, R.; May, K. *Phys. Chem. Chem. Phys.* **2000**, *2*, 943. (c) For the ruthenium atom, Ahlrichs TZVP basis set ((19s15p9d)/[8s7p5d]) as implemented in ORCA package was used.

(31) (a) Neese, F. *J. Chem. Phys.* **2001**, *115*, 11080. (b) Sinnecker, S.; Rajendran, A.; Klamt, A.; Diedenhofen, M.; Neese, F. *J. Phys. Chem. A* **2006**, *110*, 2235.

(32) (a) Neese, F. *J. Chem. Phys.* **2005**, *122*, 034107. (b) Hess, B. A.; Marian, C. M.; Wahlgren, U.; Gropen, O. *Chem. Phys. Lett.* **1996**, *251*, 365.

(33) Remenyi, C.; Kaupp, M. *J. Am. Chem. Soc.* **2005**, *127*, 11399.

(34) (a) Sinnecker, S.; Neese, F.; Noodleman, L.; Lubitz, W. *J. Am. Chem. Soc.* **2004**, *126*, 2613. (b) Pietrzyk, P.; Podolska, K.; Sojka, Z. *J. Phys. Chem. A* **2008**, *112*, 12208.

(35) Kaupp, M.; Reviakine, R.; Malkina, O. L.; Arbuznikov, A.; Schimmelpfennig, B.; Malkin, V. G. *J. Comput. Chem.* **2002**, *23*, 794.

(36) Khan, M. M. T.; Srinivas, D.; Kureshy, R. I.; Khan, N. H. *Polyhedron* **1991**, *10*, 2559.

(37) Das, A.; Peng, S.-M.; Lee, G.-H.; Bhattacharya, S. *New J. Chem.* **2004**, *28*, 712.

(38) Raveendran, R.; Pal, S. *Inorg. Chim. Acta* **2006**, *359*, 3212.

(39) Raja, N.; Ramesh, R. *Spectrochim. Acta, Part A* **2010**, *75*, 713.

(40) Patra, S.; Sarkar, B.; Mobin, S. M.; Kaim, W.; Lahiri, G. K. *Inorg. Chem.* **2003**, *42*, 6469.

(41) Yamada, H.; Koike, T.; Hurst, J. K. *J. Am. Chem. Soc.* **2001**, *123*, 12775–12780.

(42) Doppelt, P.; Meyer, T. J. *Inorg. Chem.* **1987**, *26*, 2027–2034.

(43) Maliyackel, A. C.; Walz, W. L.; Lilie, J.; Woods, R. J. *Inorg. Chem.* **1990**, *29*, 340.

(44) Boyer, J. L.; Rochford, J.; Tsai, M.-K.; Muckerman, J. T.; Fujita, E. *Coord. Chem. Rev.* **2010**, *254*, 309.